PCCP

PAPER

View Article Online
View Journal | View Issue

Cite this: *Phys. Chem. Chem. Phys.*, 2024, **26**, 6265

Early bird or night owl? Controlling the ultrafast photodynamics of triphenylamine substituted 2,2′:6′,2″-terpyridine†

Anna Maria Maroń, *[a] Oliviero Cannelli, *[bc] Etienne Christophe Socie,[b] Piotr Lodowski,[a] Malte Oppermann,[bd] Barbara Machura[a] and Majed Chergui[be]

Received 15th September 2023,
Accepted 15th January 2024

DOI: 10.1039/d3cp04492k

rsc.li/pccp

Controlling the ultrafast photodynamics of metal-free organic molecules has great potential for technological applications. In this work, we use solvent polarity and viscosity as "external knobs" to govern the photodynamics of an electron-donating derivative of 2,2′:6′,2″-terpyridine (**terpy**), namely 4′-(4-(di(4-*tert*-butylphenyl)amine)phenyl)-2,2′:6′,2″-terpyridine (***t*BuTPAterpy**). We combine femtosecond fluorescence upconversion (FlUC), transient absorption (TA) and quantum mechanical calculations to provide a comprehensive description of the ***t*BuTPAterpy**'s photodynamics. Our results demonstrate that, by changing the solvent, the time scale of light-induced conformational changes of the system can be tuned over two orders of magnitude, controlling the ***t*BuTPAterpy** fluorescence spectral region and yield. As a result, depending on the local environment, ***t*BuTPAterpy** can act either as an "early bird" or a "night owl", with a tunability that makes it a promising candidate for metal-free sensors.

Introduction

Intramolecular charge transfer (ICT) is a fundamental phenomenon responsible for a large number of chemical and biological processes in organic and inorganic systems.[1] Several investigations were devoted to ICT, which is exploited in applications for molecular electronics, solar energy-conversion, quantum optics and chemical sensors.[2–7] In addition, the fundamental understanding of ICT has fascinated scientists over the past few decades.[8–20] In ICT systems, the early photodynamics upon optical transitions to the lowest electronic states is associated with the population transfer from the locally-excited (LE) Franck–Condon (FC) region to the relaxed geometry of the ICT state.[21] These conformational changes include twisting,[9,22–27] planarization,[23,24,27–30] bending,[31] rehybridization of molecular fragments within the ICT moiety,[13,32] and/or intersystem crossing (ISC) to the triplet manifold.[33–37] Such structural and electronic changes are strongly influenced by environment effects. As a consequence, solvent parameters like polarity and viscosity can be used as experimental knobs for the external control of the ICT photodynamics.[3] A rational design of ICT devices requires characterizing their ultrafast photodynamics and quantifying the impact of solvent parameters on their photoresponse.[21]

Herein, we focus on the donor–acceptor molecule 4′-(4-(di(4-*tert*-butylphenyl)amine)phenyl)-2,2′:6′,2″-terpyridine (***t*BuTPAterpy**) shown in Fig. 1. Derivatives of 2,2′:6′,2″-terpyridine (**terpy**) are among the most important organic ligands in coordination chemistry.[38–46] Several spectroscopic investigations described the photophysical properties of transition metal complexes with **terpy** ligands,[43,46–51] showing that electron-donating substituents lengthen the photoluminescence lifetime of the compounds. This is generally due to an energy barrier increase between the emissive metal-to-ligand charge transfer triplet (^{3}MLCT) state and the metal-centred triplet (^{3}MC) state,[52–55] or to the equilibration between the ^{3}MLCT state and the intraligand triplet (^{3}ILCT/^{3}IL) state.[47,51,56,57] Despite the widespread use of **terpys** and their derivatives, the photophysics of the isolated ligands was to a great extent overlooked. Only a limited number of studies described the ultrafast photodynamics of these organic compounds,[58,59] underestimating the great potential of these metal-free systems for various applications.

[a] *Institute of Chemistry, University of Silesia, Szkolna 9, 40-007 Katowice, Poland. E-mail: anna.maron@us.edu.pl*
[b] *Laboratory of Ultrafast Spectroscopy (LSU) and Lausanne Centre for Ultrafast Science (LACUS), École Polytechnique Fédérale de Lausanne, ISIC CH H1 625, Station 6, CH-1015, Lausanne, Switzerland*
[c] *Center for Free-Electron Laser Science, DESY, Notkestraße 85, 22607 Hamburg, Germany. E-mail: oliviero.cannelli@cfel.de*
[d] *Department of Chemistry, University of Basel, Klingelbergstrasse 80, 4056 Basel, Switzerland*
[e] *Elettra – Sincrotrone Trieste S.C.p.A., S.S.14 Km.163, 5 in Area Science Park, I – 34149, Trieste, Italy*

† Electronic supplementary information (ESI) available: Details about experiments, photodamage and fluence dependence tests, comparison of time-resolved spectra to steady state spectra, DAS and EAS, and details about global fitting procedures. See DOI: https://doi.org/10.1039/d3cp04492k

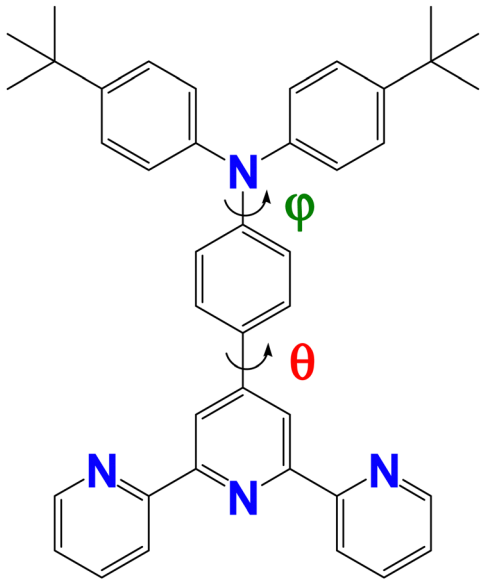

Fig. 1 Structure of 4′-(4-(di(4-*tert*-butylphenyl)amine)phenyl)-2,2′:6′,2″-terpyridine (***t*BuTPAterpy**). The dihedral angles θ and φ correspond to the torsions of the terpyridine and phenyl units, and of the phenyl and amide units, respectively.

In a recent study,[60] we investigated the steady-state properties of ***t*BuTPAterpy**, showing that it is highly sensitive to solvent polarity, viscosity and pH. These features, together with its high fluorescence quantum yield (Φ_{PL} = 0.48–0.83 and τ_{PL} = 1.53–6.56 ns), make it a potential candidate as a metal-free environment sensor. Our previous joint experimental and computational work provided a picture of ***t*BuTPAterpy**'s energy diagram, showing that the absorption process is dominated by an ICT $S_0 \rightarrow S_1$ transition, while the near-lying $S_0 \rightarrow S_2$ transition has an oscillator strength several orders of magnitude lower. However, fully exploiting the applicative potentials of this system requires a better understanding of how the environment influences its early photodynamics, which governs its final emission properties. In this work, we performed a detailed study of the ***t*BuTPAterpy** ultrafast photoresponse using femtosecond fluorescence upconversion (FlUC), femtosecond transient absorption (TA) spectroscopy, and quantum chemical calculations, rationalizing solvent polarity and viscosity effects on the system's photophysics. In chloroform, we show that at least three conformers participate in the deactivation pathways of the molecule. Increasing the solvent polarity leads to a barrier-less motion that activates a conformational change to the lowest energy excited state on sub-ps time scales, while higher solvent viscosities slow down the process up to hundreds of ps. Finally, in the absence of strong polarity and viscosity effects, the ISC to the triplet manifold becomes the dominant process.

Experimental and computations

Materials

***t*BuTPAterpy** was obtained according to the procedure described in ref. 51. Analytical data for ***t*BuTPAterpy** (^{1}H and ^{13}C NMR spectroscopy and elemental analysis) are reported in the ESI,† and are in good agreement with those discussed in ref. 51. All solvents were of spectroscopic grade (chloroform, *n*-hexane, and glyceryl triacetate) or HPLC grade (acetonitrile, water impurities $<0.02\%$) and were commercially available (Merck, Karl–Fischer).

Measurement techniques, sample preparation and method of analysis

FlUC and TA spectroscopy studies were conducted using the setups described in ref. 61 and 62, and additional details are reported in the ESI.† Quartz cuvettes of 2 mm (TA) and 1 mm (FlUC) thicknesses were used for sample solutions having concentrations of 125 μM and 250 μM, respectively. The stability of ***t*BuTPAterpy** in chloroform, acetonitrile, glycerol triacetate and *n*-hexane was spectrophotometrically monitored over 48 hours prior to the analysis (Fig. S1, ESI†). Photostability experiments and fluence dependence characterizations are reported in Fig. S2 and S3 (ESI†), respectively.

The FlUC setup consists of a Ti:sapphire laser (Libra, Coherent, 800 nm central wavelength, 45 fs pulse duration, and 1 kHz repetition rate) and a FlUC spectrofluorimeter (LIOP-TEC). 400 nm excitation pulses were produced by doubling the 800 nm light with a I type BBO crystal (d = 0.5 mm). The sample solution was excited in the magic angle geometry (54.7°). The type II sum-frequency generation was obtained from the horizontally polarized gate beam and the vertically polarized fluorescence. The upconverted light was collected using an unfolded Czerny–Turner spectrograph and detected using a CCD camera (Newton 920, Andor). The instrument response function (IRF) of the measurements was estimated from the full widths at half maximum (FWHM) of the cross-correlation signal of the pump and probe pulses, corresponding to 0.140 ps and 0.150 ps, respectively for $CHCl_3$ and acetonitrile solutions.

The TA spectra were measured using a Helios setup (Ultrafast Systems) equipped with a femtosecond Ti:sapphire regenerative amplified laser system (Astrella, Coherent, 800 nm central wavelength, 1 kHz repetition rate). A CaF_2 crystal and an optical parametric amplifier (Light Conversion, TOPAS prime) were used for the generation of the white light probe and the 405 nm pump beam, respectively. A CCD detector was used to collect the TA signal in transmission geometry. The IRF was measured in pure solvents (FWHM of about 160 fs, 150 fs, 150 fs, 150 fs were measured in $CHCl_3$, glyceryl triacetate, acetonitrile, *n*-hexane, respectively).

The Surface Xplorer (Ultrafast Systems) software was employed for the data processing of the TA data sets. The analysis of FlUC and TA data sets was performed using the Optimus™ software.[63] A detailed description of the data analysis procedure is given in the ESI.†

Computational details

All calculations were performed at the density-functional theory (DFT)[64] and time-dependent density-functional theory (TD-DFT)[65] level, using the hybrid Perdew–Burke–Ernzerhof (PBE0) functional[66,67] and the def2-SVP basis set.[68] Solvation effects on the system's geometry and electronic structure were included by

using a polarizable continuum model (PCM).[69] The geometry of the ground state (S_0) was fully optimized without any structural parameter constraints. The geometries of the excited states were determined using TD-DFT without (S_1) and with (S_2) structural constraints on the dihedral **terpy**-phenil angle (θ).

Results and discussion

FlUC and TA of ***t*BuTPAterpy** were measured in both $CHCl_3$ (ε = 4.81 and η = 0.51 cP) and acetonitrile (ε = 37.5 and η = 0.34 cP), while TA data were further collected varying the solvent polarity and viscosity, respectively, measuring the system in *n*-hexane (ε = 1.88, η = 0.28 cP), and glyceryl triacetate (triacetine, ε = 7.01, η = 25 cP).[70–72] The results are summarized in Table 1, in Fig. 2 (FlUC in $CHCl_3$) and in Fig. 3–6 (TA in all solvents), and are discussed in more detail hereafter. Additional information is reported in Fig. S4–S14 in the ESI.†

Table 1 FlUC and TA decay lifetimes (ps) of ***t*BuTPAterpy** in the investigated solvents obtained from the global fit analysis

	FlUC		TA				
	$CHCl_3$	CH_3CN		$CHCl_3$	CH_3CN	*n*-Hexane	Triacetine
τ_1	0.31	0.23	τ_1	0.54	0.20	—	0.67
τ_2	3.7	1.2	τ_2	3.1	1.4	—	10
τ_3	9.8	—	τ_3	8.9	—	—	110
τ_4	—	—	τ_4	210	110	72	560
τ_5	Infinite	Infinite	τ_5	4400	5800	1600	4800
τ_6	—	—	τ_6	—	—	Infinite	—

Femtosecond studies in chloroform.

The FlUC results of ***t*BuTPAterpy** in $CHCl_3$ are shown in Fig. 2 (see also Fig. S4 and S5 in the ESI†). Within the first 10 ps of the dynamics, the fluorescence signal grows and shifts towards lower energies and decays at longer time scales (Fig. 2A and B). The emission band centred at $\sim$21 740 cm^{-1} (460 nm), which promptly appears after the pump pulse, largely overlaps with the steady-state emission spectrum of ***t*BuTPAterpy** at 77 K (see Fig. S4, panel D, ESI†). Instead, the band after 1000 ps time delay, which is centred at $\sim$20 410 cm^{-1} (490 nm), matches well with the steady-state emission spectrum at room temperature (Fig. S4, panel D, ESI†). Time-resolved area normalized emission spectra (TRANES, Fig. 2C) show a quasi-isoemissive point at $\sim$21 000 cm^{-1} (475 nm) for time delays longer than 10 ps, pointing to the presence of two transient emitting states.[20,73–78]

To obtain further insights into the relaxation dynamics of ***t*BuTPAterpy**, a global lifetime analysis of the FlUC data was performed, with the best fit achieved using a four-component exponential decay model. Three-component fits were attempted without reaching a satisfactory agreement with the experiment, whereas adding a fifth component to the four-component fit did not provide significant improvements, as shown in Fig. S15 in the ESI.† The two shortest components, τ_1 and τ_2, respectively of 0.31 ps and 3.7 ps, agree well with the inertial (0.285 ps) and diffusional (4.15 ps) solvation processes in chloroform for coumarin153,[79] while the longer time constants τ_3 and τ_4 are ascribed to solute kinetics. These results are complemented and confirmed by the TA measurements presented in the following.

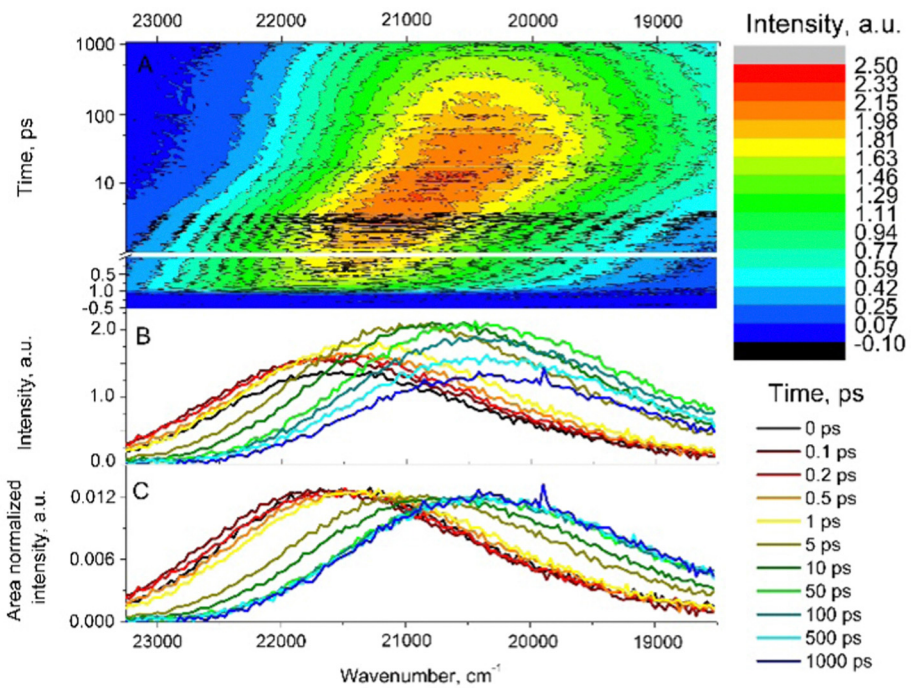

Fig. 2 FlUC data for ***t*BuTPAterpy** in chloroform solution (λ_{exc} = 400 nm): 2D time-wavenumber plot (A); FlUC spectra at selected time delays (B); and TRANES (C). The time axis break at 1 ps separates linear and logarithmic ranges.

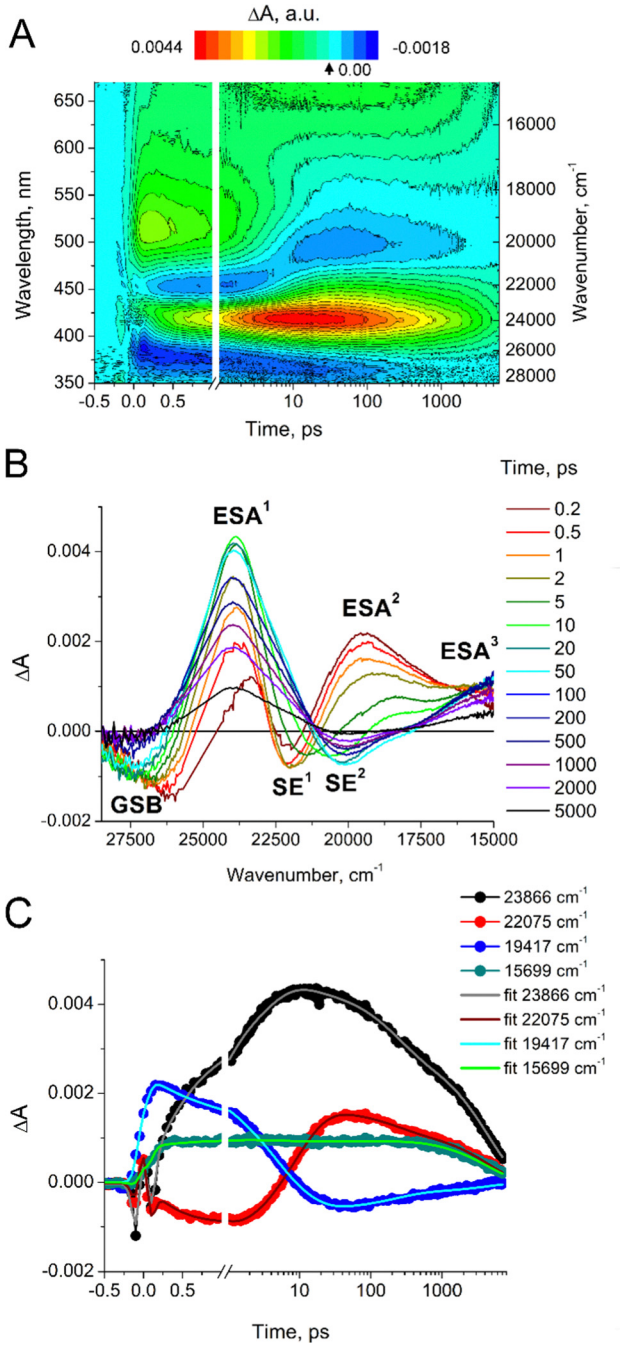

Fig. 3 TA 2D maps (panel A), TA spectra at selected time delays (panel B), selected time traces with their fits (panel C) for ***t*BuTPAterpy** in $CHCl_3$ (λ_{exc} = 405 nm). The time axis break at 1 ps separates linear and logarithmic ranges. The arrow in the color bar of panel A indicates the 0 OD value of the transient absorption.

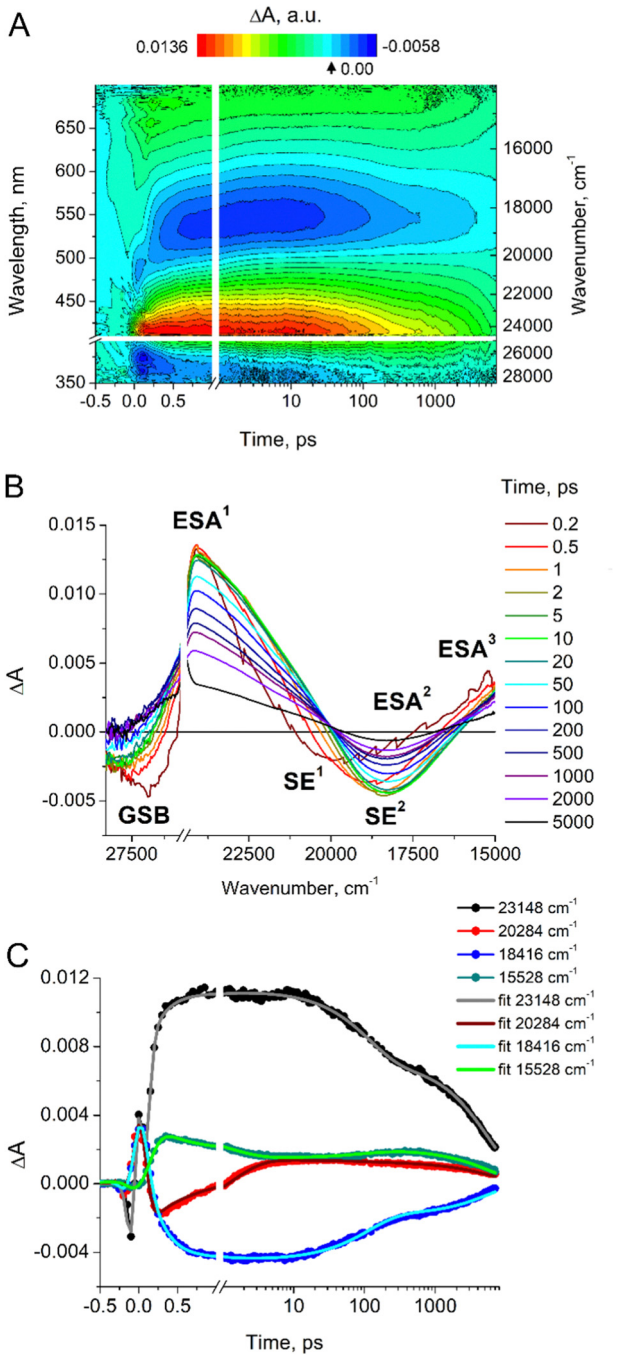

Fig. 4 TA 2D maps (panel A), TA spectra at selected time delays (panel B), selected time traces with their fits (panel C) for ***t*BuTPAterpy** in acetonitrile (λ_{exc} = 405 nm). The time axis break at 1 ps separates linear and logarithmic ranges, whereas the axis break at 25 316–24 390 cm^{-1} (395–410 nm) corresponds to the photon energy of the Raman scattering line of the acetonitrile solvent and was excluded from the analysis. The arrow in the color bar of panel A indicates the 0 OD value of the transient absorption.

Fig. 3A shows the TA signal of ***t*BuTPAterpy** in $CHCl_3$. On sub-ps time scales, it consists of two negative and two positive alternating regions. The negative features correspond to a ground-state bleaching (GSB) in the energy range 28 600–25 000 cm^{-1} (350–400 nm) and to a stimulated emission band (SE^1) lying between 22 700 cm^{-1} (441 nm) and 20 800 cm^{-1} (481 nm). The latter overlaps well with the fluorescence spectra at short time scales of Fig. 2. The two positive bands are related to excited state absorption (ESA) processes and lie at 25 000–22 700 cm^{-1} (400–441 nm, ESA^1) and 20 800–16 700 cm^{-1} (481–599 nm, ESA^2). Within 1 ps after excitation, a third band (ESA^3) appears between 16 700 cm^{-1} (599 nm) and 14 900 cm^{-1}

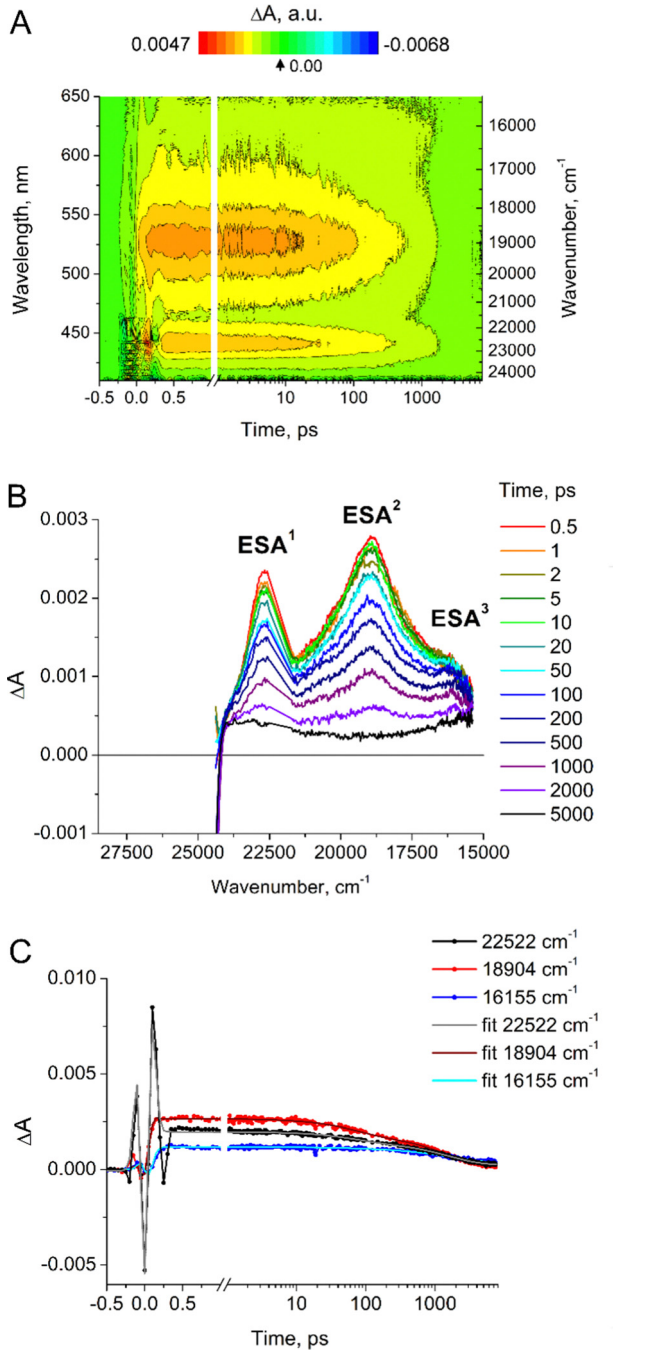

Fig. 5 TA 2D maps (panel A), TA spectra at selected time delays (panel B), selected time traces with their fits (panel C) for ***t*BuTPAterpy** in *n*-hexane (λ_{exc} = 405 nm). The time axis break at 1 ps separates linear and logarithmic ranges. The arrow in the color bar of panel A indicates the 0 OD value of the transient absorption.

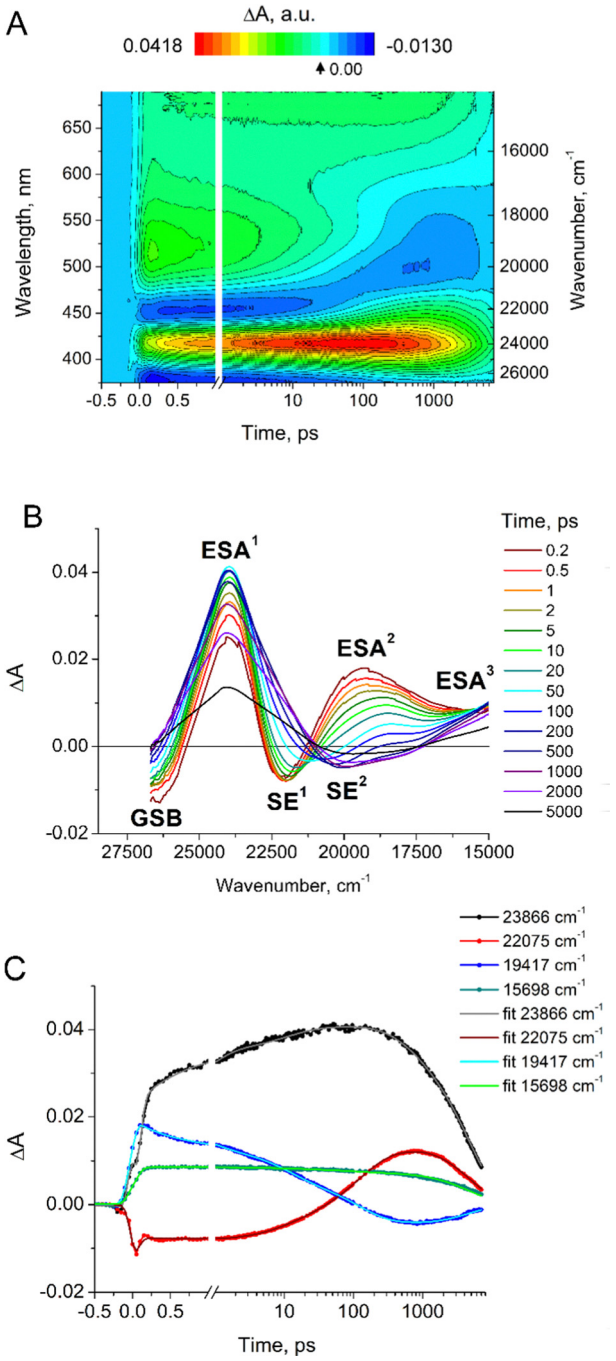

Fig. 6 TA 2D maps (panel A), TA spectra at selected time delays (panel B), selected time traces with their fits (panel C) for ***t*BuTPAterpy** in glyceryl acetate (λ_{exc} = 405 nm). The time axis break at 1 ps separates linear and logarithmic ranges. The arrow in the color bar of panel A indicates the 0 OD value of the transient absorption.

(671 nm). The SE^1 band grows during the first 2 ps and red-shifts into a new band (SE^2) at longer time delays. The presence of an isoemissive point at 21 050 cm^{-1} (475 nm) supports the assignment of these emission bands to two different transient species. The ESA^2 band grows within the IRF and starts decaying on a sub-ps time scale. As reported for similar π-conjugate structures,[58,59] we assign it to $S^1 \rightarrow S^n$ transitions within the **terpy** moiety. The narrow and intense ESA^1 band is typical of polypyridine anion radicals[80] in free organic ligands and their metal coordination compounds.[81–84] Instead, the ESA^3 band is ascribed to the cation radical species of the donor unit.[85] The coexistence of ESA^1 and ESA^3 transient signals respectively corresponding to anion and cation radicals is consistent with a photoinduced ICT process. The experimental results

are satisfactorily reproduced using a five-component global target analysis (see Table 1, and also Fig. S6 and S17 in the ESI† for a complete set of time traces and for the map of residuals). The obtained time constants are in good agreement with the FlUC analysis, with the notable exception for the presence of an additional time constant of 210 ps in the TA fit (Table 1). Based on the analysis of the TA spectra at different time delays, we conclude the following:

(i) The GSB and all ESA features start growing within the IRF of the experiment;

(ii) The first component with a lifetime of τ_1 = 0.54 ps is related to the formation of SE^1 and a partial growth (decay) of ESA^1 (ESA^2). These signals reflect the formation of an S_1 excited state having a moderate ICT character and populating the lowest unoccupied molecular orbital (LUMO) centred on the **terpy** moiety.[60] At these time scales, the SE^1 band and the FlUC signal are blue-shifted with respect to the room temperature emission spectrum. As discussed in ref. 60, this is typical of the ***t*BuTPAterpy** system in the absence of structural changes with respect to the FC geometry;

(iii) The time constant τ_2 (3.1 ps) is associated with a progressive red shift and intensity drop of the SE^1 and ESA^2 bands, and a further growth of the ESA^1 band;

(iv) During τ_3 (8.9 ps), the ESA^1 band keeps growing, whereas the SE^1 band red shifts towards the newly formed SE^2 band, giving rise to the isoemissive point at 21 050 cm^{-1} (475 nm). During τ_2 and τ_3, the system undergoes a relaxation process towards a molecular configuration having an emission spectrum compatible with room temperature fluorescence (see Fig. S4, panel D, ESI†). This observation, together with the presence of the ESA^1 and ESA^3 bands, is consistent with the formation of an ICT state upon conformational changes of the molecular moieties;[60]

(v) The τ_4 time component (210 ps) is mostly associated with the decay of the ESA^1 and SE^2 features;

(vi) The τ_5 time constant of 4.4 ns agrees with the photoluminescence decay times measured in Time-correlated Single Photon Counting (TCSPC, 4.3 ns)[60] and therefore corresponds to the radiative decay of the final excited state.

Fig. S5 and S6 in the ESI† show the comparison of absorption, emission and excitation steady-state spectra of ***t*BuTPAterpy** in $CHCl_3$ with FlUC and TA energy traces at multiple time delays, and TA time traces with their fits, respectively.

Femtosecond studies in acetonitrile and *n*-hexane.

The comparison of TA experiments in solvents of higher (acetonitrile) and lower (*n*-hexane) polarity with respect to the moderately polar $CHCl_3$ provides a better understanding of how the solvent polarity affects the photodynamics of the push–pull ***t*BuTPAterpy** molecule (Fig. 4 and 5).

In acetonitrile (Fig. 4), the TA spectral shapes resemble those in chloroform, showing only a minor hypsochromic shift of the ESA^1 band and a bathochromic shift of the SE^2 band. However, differently from chloroform, the best fit of the TA global target analysis was achieved with a four-component model (see Fig. S8 and S18, ESI†). In this case, the spectral changes from the SE^1 to the SE^2 band occur almost immediately after photoexcitation, giving rise to an isoemissive point at 20 040 cm^{-1} (499 nm) between the traces at 0.2 and 0.5 ps (Fig. 4B). The τ_1 and τ_2 components approximately agree with the time constants previously reported for the solvation dynamics of coumarin153 in acetonitrile.[79] Thus, if a population transfer occurs between two different emitting states, it overlaps with the sub-ps inertial solvation process, explaining the absence of a fifth time component in the fit with respect to the chloroform data set. This observation agrees with the TRANES results of the FlUC measurements in acetonitrile, where no isoemissive point is observed (Fig. S9, ESI†) and where the transient spectral shifts are typical of solvation dynamics time scales. Similar to chloroform, in acetonitrile the TA fit of ***t*BuTPAterpy** requires one additional component (four) with respect to the FlUC data (three), as reported in Table 1, and the longest time component matches well the decay time of the TCSPC measurements.[60]

In the non-polar *n*-hexane, the transient signal intensity is significantly lower than that in the polar solvents under similar pump fluences. This is a consequence of the hypsochromic shift of the steady-state ***t*BuTPAterpy** absorption onset, which leads to a lower sample absorbance at 24 690 cm^{-1} (405 nm). Compared to chloroform, both ESA^1 and ESA^2 bands are bathochromically shifted by about 500–1300 cm^{-1}, while a hypsochromic shift of $\sim$950 cm^{-1} is observed in the case of ESA^3 band. The SE^1 band at 24 570 cm^{-1} (407 nm)[60] partially overlaps with the pump signal and is buried under the stronger ESA^1 band, resulting in a positive feature of the TA map (see Fig. S11 for the comparison of TA spectra with the steady-state spectra in *n*-hexane, ESI†). The global lifetime analysis of the *n*-hexane data was performed using three components (see Table 1, Fig. 5C, and Fig. S12 in the ESI,† which show the details of the global analysis in *n*-hexane). Both the first and second time constants correspond to a decay of the positive signal, with the latter closely resembling the PL decay time in *n*-hexane (1.53 ns).[60] By comparing the results in *n*-hexane and $CHCl_3$, a remarkable difference is the presence of a persisting signal up to the longest measured delays in *n*-hexane. This ''slow'' component is characteristic of the ESA^1 and ESA^3 bands only, which have maxima respectively at 23 810 cm^{-1} (420 nm) and $<$15 400 cm^{-1} ($>$649 nm). Instead, the ESA^2 band disappears at about 5000 ps time delay. In the ns time delay range, the transients agree with the triplet–triplet ESA bands of the TA spectra of TPA-substituted benzimidazole derivatives, as reported in ref. 37.

Femtosecond studies on glyceryl acetate

The TA 2D map of ***t*BuTPAterpy** in the viscous triacetine solvent is reported in Fig. 6 (panel A). The spectral profiles resemble the TA spectra in $CHCl_3$: the ESA bands are in the same energy range, and the SE^1 and SE^2 bands undergo similar spectral changes. The position of the SE^2 band agrees with the steady-state emission spectrum of ***t*BuTPAterpy** in the triacetine solvent (see Fig. S13 in the ESI†), and the 2D map is satisfactorily fitted using a five-component model. However, with respect to

$CHCl_3$, the system's photodynamics significantly slows down upon the increase of solvent viscosity (see Table 1 and Fig. S14, S20 in the ESI† for details about the global analysis). The highest increase concerns τ_3, which is one order of magnitude larger in triacetine than in chloroform, suggesting that this time constant corresponds to a conformational change of the solute. The isoemissive point at 20 880 cm^{-1} (479 nm) further suggests the presence of two emissive states. Instead, the τ_5 component matches the decay time observed in the TCSPC measurement.[60] Minor differences between the two solvents are also present, as the absence of an initial blue shift of the ESA^1 band and a fast growth of the SE^1 band within τ_1 (not within τ_2, as it happens in chloroform).

Excited state kinetics of *t*BuTPAterpy

Combining the experimental results reported in the previous sections with DFT calculations, we propose in Fig. 7 the energy diagram describing the ***t*BuTPAterpy**'s photodynamics in $CHCl_3$. In the ground state, ***t*BuTPAterpy** is characterized by an equilibrium structure where its building blocks lie in different planes forming dihedral angles of $\theta = 26^\circ$ (terpy-phenyl angle) and $\phi = 33^\circ$ (phenyl-amide angle).[60] The excitation at 405 nm initially populates the S_1 excited state, which in the FC geometry has a moderate intramolecular charge transfer character (ICT_1).[60] Our experimental evidences show that the inertial and diffusive solvation processes, which are responsible for the first two time components of the photodynamics, lead to a Stokes shift of the emissive band, consistently with an energy stabilization of the ICT_1 state. The third relaxation process, which is strongly affected by the solvent viscosity (see triacetine results), is ascribed to conformational changes of the system towards geometries at lower energy with respect to the FC region.

We elucidated these structural modifications by performing excited-state optimisations at the TD-DFT level. The calculations highlight that the torsions along the θ and φ dihedral angles have high influence on the system's energy.[60] In particular, the energy minimum of the S_1 state (ICT_1') is reached for φ and θ approaching 53° and 2°, respectively (Fig. 7, left structure). This is due to the fact that the planarization of the θ angle stabilizes the LUMO, which was shown to span over the **terpy** and central phenyl units.[60] For the same reason, increasing θ destabilizes the first excited state, while it marginally affects the second non-emissive excited state (ICT_2), whose LUMO+1 occupied orbital was reported to be solely localised on the **terpy** substituent.[60] As a consequence, the torsion along θ causes a change in the relative energy of the first bright and second dark excited states, with an energy barrier of only few kcal mol^{-1} between them.[60] This energy separation is of the same order of magnitude of the energy dissipated by the system in the relaxation dynamics, as observed through the red shift of the ***t*BuTPAterpy** transient emission spectra within the first 10 ps. Therefore, it is reasonable to assume that during the third relaxation process (τ_3) two different excited-state conformers, ICT_1' and ICT_2, are populated (Fig. 7). Considering that the potential energy surface of the ICT_2 along the θ coordinate

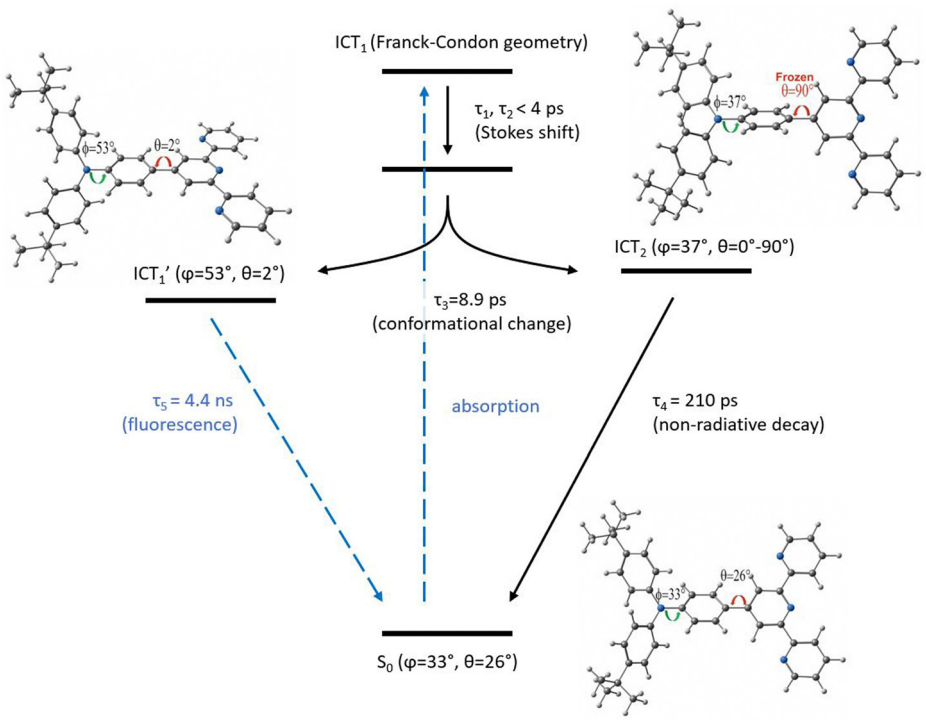

Fig. 7 Schematic of the excited state dynamics of ***t*BuTPAterpy** in $CHCl_3$. The dihedral angles θ and φ correspond to the rotations of the bonds connecting the **terpy**-phenyl and phenyl-amide, respectively. The S_0 and ICT_1' structures correspond to the optimized geometries of the ground and first excited state, respectively. The ICT_2 structure was obtained by optimising the geometry of the excited state under the constraint of $\theta = 90^\circ$.

is approximately flat,[60] the energy minimum of this state is mostly defined by the torsion along the φ dihedral angle. Thus, even though unconstrained structural optimisations of the ICT_2 state cannot be performed at the TD-DFT level, we could estimate its minimum-energy geometry along the φ coordinate in the case of θ frozen at 90° (Fig. 7, right structure), a value at which the first two excited states change in relative order.[60]

A population transfer towards a new conformer is consistent with the presence of an isoemissive point in both TRANES and SE bands. We ascribe the ICT_1' state to the long living emissive state of ***t*BuTPAterpy**, as confirmed by the overlap of the late FlUC transient emission spectrum and the room temperature fluorescence signal (see Fig. S4, ESI†). Furthermore, the ICT_1' emission decays in few ns, in agreement with the time scales observed in the TCSPC experiment.[60] The hypothesis of a small fraction of photoexcited ***t*BuTPAterpy** in a non-radiative state (ICT_2), which is populated alternatively to the ICT_1' conformer during τ_3, is supported by the presence of the second-to-last time constant of the TA experiments. We interpret this 210 ps (560 ps) decay component in $CHCl_3$ (triacetine) as a non-radiative decay from the ICT_2 to the ground state, compatibly with its absence in the FlUC experiment.

Changes in the solvent lead to modifications of the early photodynamics of ***t*BuTPAterpy**. For instance, the rate of the conformational change of the system is modulated by changing the viscosity while keeping the same polarity. Hence, in the viscous triacetine we observe a lengthening of the time components ascribed to population transfers between ICT_1 and the excited-state minima ICT_1' and ICT_2, and to the relaxation of the ICT_2 to the ground state. More polar environments facilitate the formation of the ICT_1' state, stabilizing it and lowering the conformational energy barrier with the initially populated ICT_1 state, similarly to what was reported for push–pull pyridium salts by Carlotti *et al.*[86] Thus, in the highly polar acetonitrile, the ***t*BuTPAterpy** photodynamics is solvation-controlled, while in the moderately polar $CHCl_3$ it is controlled by the slower conformational changes.

Finally, since a pronounced solvent polarity is required for the stabilization of the CT states, the apolar *n*-hexane favours a different relaxation pathway over the population transfer towards new conformers, namely an ISC process to the triplet manifold. The ICT_1 (S_1) → LE (T_n) process, which is allowed by the El-Sayed rule, was previously observed in apolar solvents in the case of 2,6-bis(diphenylamino)anthraquinone.[36] In the specific case of the push–pull ***t*BuTPAterpy** system, the population of the initially formed ICT_1 (S_1) singlet state in the FC geometry is directly transferred to the LE (T_1) triplet state localized on the 4-(di(4-*tert*-butylphenyl)amine)phenyl moiety before the structural change to the ICT_1' conformer occurs, a process which is possibly slowed down by a high conformational energy barrier.

Conclusions

In this work, we characterized the ultrafast photodynamics of the push–pull molecule ***t*BuTPAterpy**, rationalizing the solvent polarity- and viscosity-dependence of its steady-state properties that we analysed in our previous study.[60] Based on DFT calculations, and FlUC and TA measurements as a function of solvent properties, we proposed a diagram describing the system's relaxation dynamics in $CHCl_3$, showing the presence of multiple transient ICT conformers. Upon photoexcitation, the ***t*BuTPAterpy** populates a singlet state (ICT_1) which undergoes energy stabilization due to solvent relaxation processes. Within 10 ps, a structural change involving the torsions of the terpy, phenyl and amide units along the θ and φ dihedral angles leads to a population transfer to a second emitting conformer, ICT_1', which decays to the ground state through a fluorescence channel occurring in the ns time scales. We also determined the presence of a second "dark" ICT conformer (ICT_2), populated alternatively to the ICT_1 state and undergoing non-radiative decay to the ground state.

By combining ultrafast measurements as a function of solvent polarity and viscosity, we corroborated the interpretation proposed in the energy diagram and explained how the environment influences the ***t*BuTPAterpy** photodynamics. Specifically, increasing the solvent viscosity slows down the ICT_1 → ICT_1' conformational change of about one order of magnitude, as observed in ***t*BuTPAterpy** in glyceryl triacetate. Conversely, a solvent polarity increase reduces the energy barrier of the ICT_1 → ICT_1' conformational change, speeding up a population transfer process which occurs on sub-ps time scales in acetonitrile. Instead, by minimizing the solvent polarity effects, as in the case of apolar *n*-hexane, a parallel pathway involving ISC is favoured. In this solvent, the ICT_1 (S_1) → LE (T_n) decay is the dominant relaxation channel and it occurs on shorter time scales than the conformational change.

Overall, this study reveals the complexity of ***t*BuTPAterpy** photodynamic as a representative example of push–pull derivatives of 2,2′:6′,2″-terpyridine. Even though these ligands are mostly used as building blocks in coordination chemistry for the enhancement of photoluminescence yields in metal complexes, our work stresses the potential of **terpy** derivatives as metal-free environment probes whose photodynamics can be easily controlled through external solvent parameters. The reported ultrafast investigation confirms that ***t*BuTPAterpy** is a promising candidate for sensing applications, and it provides a fundamental understanding of its excited state dynamics, laying the foundations for chemical and technological optimisations of metal-free sensors.

Author contributions

Conceptualisation: A. M. M., O. C. and M. C.; methodology: A. M. M., O. C., P. L. and M. O.; software: A. M. M. and P. L.; validation: A. M. M., O. C. and B. M.; formal analysis: A. M. M., O. C., P. L. and E. C. S.; investigation: A. M. M. and E. C. S.; resources: A. M. M., B. M. and M. C.; data curation: A. M. M., O. C., P. L. and E. C. S.; writing—original draft preparation: A. M. M., O. C. and B. M.; writing—review and editing: A. M. M., O. C., M. O., B. M. and M. C.; visualisation: A. M. M., O. C., P. L.

and M. C.; supervision: A. M. M. and M. C.; project administration: A. M. M.; funding acquisition: A. M. M, B. M. and M. C. All authors have read and agreed to the published version of the manuscript.

Conflicts of interest

There are no conflicts to declare.

Acknowledgements

This research was funded by the National Science Centre of Poland, SONATA grant no. 2020/39/D/ST4/00286. The research activities were co-financed by the funds granted under the Research Excellence Initiative of the University of Silesia in Katowice. This work was supported by the ERC *via* the DYNAMOX and CHIRAX advanced grants, and the Swiss SNF *via* the NCCR:MUST. AMM thanks the Polish National Agency for Academic Exchange (PPN/BEK/2018/1/00275/U/00001).

Notes and references

1 M. Hao, W. Chi, C. Wang, Z. Xu, Z. Li and X. Liu, Molecular Origins of Photoinduced Backward Intramolecular Charge Transfer, *J. Phys. Chem. C*, 2020, **124**, 16820–16826.
2 M. Ratner, A brief history of molecular electronics, *Nat. Nanotechnol.*, 2013, **8**, 378–381.
3 S. Sasaki, G. P. C. Drummen and G. Konishi, Recent advances in twisted intramolecular charge transfer (TICT) fluorescence and related phenomena in materials chemistry, *J. Mater. Chem. C*, 2016, **4**, 2731–2743.
4 V. Malytskyi, J.-J. Simon, L. Patrone and J.-M. Raimundo, Thiophene-based push–pull chromophores for small molecule organic solar cells (SMOSCs), *RSC Adv.*, 2015, **5**, 354–397.
5 A. M. El-Zohry and M. Karlsson, Gigantic Relevance of Twisted Intramolecular Charge Transfer for Organic Dyes Used in Solar Cells, *J. Phys. Chem. C*, 2018, **122**, 23998–24003.
6 K. Nakayama, T. Okura, Y. Okuda, J. Matsui, A. Masuhara, T. Yoshida, M. S. White, C. Yumusak, P. Stadler, M. Scharber and N. S. Sariciftci, Single-Component Organic Solar Cells Based on Intramolecular Charge Transfer Photoabsorption, *Materials*, 2021, **14**, 1200.
7 H. Y. Chung, J. Oh, J.-H. Park, I. Cho, W. S. Yoon, J. E. Kwon, D. Kim and S. Y. Park, Spectroscopic Studies on Intramolecular Charge-Transfer Characteristics in Small-Molecule Organic Solar Cell Donors: A Case Study on ADA and DAD Triad Donors, *J. Phys. Chem. C*, 2020, **124**, 18502–18512.
8 F. Bureš, Fundamental aspects of property tuning in push–pull molecules, *RSC Adv.*, 2014, **4**, 58826–58851.
9 Z. R. Grabowski, K. Rotkiewicz and W. Rettig, Structural Changes Accompanying Intramolecular Electron Transfer: Focus on Twisted Intramolecular Charge-Transfer States and Structures, *Chem. Rev.*, 2003, **103**, 3899–4032.
10 G. L. Closs and J. R. Miller, Intramolecular Long-Distance Electron Transfer in Organic Molecules, *Science*, 1988, **240**, 440–447.
11 M. Park, C. H. Kim and T. Joo, Multifaceted Ultrafast Intramolecular Charge Transfer Dynamics of 4-(Dimethylamino)benzonitrile (DMABN), *J. Phys. Chem. A*, 2013, **117**, 370–377.
12 P. B. Coto, L. Serrano-Andrés, T. Gustavsson, T. Fujiwara and E. C. Lim, Intramolecular charge transfer and dual fluorescence of 4-(dimethylamino)benzonitrile: ultrafast branching followed by a two-fold decay mechanism, *Phys. Chem. Chem. Phys.*, 2011, **13**, 15182.
13 K. A. Zachariasse, S. I. Druzhinin, S. A. Kovalenko and T. Senyushkina, Intramolecular charge transfer of 4-(dimethylamino)benzonitrile probed by time-resolved fluorescence and transient absorption: No evidence for two ICT states and a $\pi\sigma^*$ reaction intermediate, *J. Chem. Phys.*, 2009, **131**, 224313.
14 S. I. Druzhinin, N. P. Ernsting, S. A. Kovalenko, L. P. Lustres, T. A. Senyushkina and K. A. Zachariasse, Dynamics of Ultrafast Intramolecular Charge Transfer with 4-(Dimethylamino)benzonitrile in Acetonitrile, *J. Phys. Chem. A*, 2006, **110**, 2955–2969.
15 M. A. Kochman, B. Durbeej and A. Kubas, Simulation and Analysis of the Transient Absorption Spectrum of 4-(*N*, *N* -Dimethylamino)benzonitrile (DMABN) in Acetonitrile, *J. Phys. Chem. A*, 2021, **125**, 8635–8648.
16 M. A. Kochman and B. Durbeej, Simulating the Nonadiabatic Relaxation Dynamics of 4-(*N*, *N* -Dimethylamino)-benzonitrile (DMABN) in Polar Solution, *J. Phys. Chem. A*, 2020, **124**, 2193–2206.
17 I. Gómez, P. J. Castro and M. Reguero, Insight into the Mechanisms of Luminescence of Aminobenzonitrile and Dimethylaminobenzonitrile in Polar Solvents. An ab Initio Study, *J. Phys. Chem. A*, 2015, **119**, 1983–1995.
18 I. Georgieva, A. J. A. Aquino, F. Plasser, N. Trendafilova, A. Köhn and H. Lischka, Intramolecular Charge-Transfer Excited-State Processes in 4-(*N*, *N* -Dimethylamino)-benzonitrile: The Role of Twisting and the $\pi\sigma^*$ State, *J. Phys. Chem. A*, 2015, **119**, 6232–6243.
19 A. Perveaux, P. J. Castro, D. Lauvergnat, M. Reguero and B. Lasorne, Intramolecular Charge Transfer in 4-Aminobenzonitrile Does Not Need the Twist and May Not Need the Bend, *J. Phys. Chem. Lett.*, 2015, **6**, 1316–1320.
20 A. S. R. Koti and N. Periasamy, Time resolved area normalized emission spectroscopy (TRANES) of DMABN confirms emission from two states, *Res. Chem. Intermed.*, 2002, **28**, 831–836.
21 B. Patrizi, C. Cozza, A. Pietropaolo, P. Foggi and M. Siciliani de Cumis, Synergistic Approach of Ultrafast Spectroscopy and Molecular Simulations in the Characterization of Intramolecular Charge Transfer in Push-Pull Molecules, *Molecules*, 2020, **25**, 430.
22 Z. Szakács, S. Rousseva, M. Bojtár, D. Hessz, I. Bitter, M. Kállay, M. Hilbers, H. Zhang and M. Kubinyi, Experimental

evidence of TICT state in 4-piperidinyl-1,8-naphthalimide – a kinetic and mechanistic study, *Phys. Chem. Chem. Phys.*, 2018, **20**, 10155–10164.

23 G. Haberhauer, Planarized and Twisted Intramolecular Charge Transfer: A Concept for Fluorophores Showing Two Independent Rotations in Excited State, *Chem. – Eur. J.*, 2017, **23**, 9288–9296.

24 G. Haberhauer, R. Gleiter and C. Burkhart, Planarized Intramolecular Charge Transfer: A Concept for Fluorophores with both Large Stokes Shifts and High Fluorescence Quantum Yields, *Chem. – Eur. J.*, 2016, **22**, 971–978.

25 R. Ghosh, A. Nandi and D. K. Palit, Solvent sensitive intramolecular charge transfer dynamics in the excited states of 4-N,N-dimethylamino-4′-nitrobiphenyl, *Phys. Chem. Chem. Phys.*, 2016, **18**, 7661–7671.

26 E. Benassi, B. Carlotti, M. Segado, A. Cesaretti, A. Spalletti, F. Elisei and V. Barone, Presence of Two Emissive Minima in the Lowest Excited State of a Push–Pull Cationic Dye Unequivocally Proved by Femtosecond Up-Conversion Spectroscopy and Vibronic Quantum-Mechanical Computations, *J. Phys. Chem. B*, 2015, **119**, 6035–6040.

27 Z. Zhang, G. Zhang, J. Wang, S. Sun and Z. Zhang, The mechanisms of Large Stokes Shift and Fluorescence Quantum Yields in anilino substituted Rhodamine analogue: TICT and PICT, *Comput. Theor. Chem.*, 2016, **1095**, 44–53.

28 R. Ghosh, A. Nandi, A. Kushwaha and D. Das, Ultrafast Conformational Relaxation Dynamics in Anthryl-9-benzothiazole: Dynamic Planarization Driven Delocalization and Protonation-Induced Twisting Dynamics, *J. Phys. Chem. B*, 2019, **123**, 5307–5315.

29 T. Staněk, M. Dvořák, N. Almonasy, M. Nepraš, I. Šloufová and M. Michl, Formation of planarized intramolecular charge-transfer state in dichlorotriazinyl-pyrene fluorescent probe: TD-DFT and resonance Raman study, *Dyes Pigm.*, 2017, **141**, 121–127.

30 K. A. Zachariasse, S. I. Druzhinin, W. Bosch and R. Machinek, Intramolecular Charge Transfer with the Planarized 4-Aminobenzonitrile 1- *tert* -Butyl-6-cyano-1,2,3,4-tetrahydroquinoline (NTC6), *J. Am. Chem. Soc.*, 2004, **126**, 1705–1715.

31 Q. Wu, J. Liu, Y. Li, M. M. S. Lee, L. Hu, Y. Li, P. Zhou, D. Wang and B. Z. Tang, Janus luminogens with bended intramolecular charge transfer: Toward molecular transistor and brain imaging, *Matter*, 2021, **4**, 3286–3300.

32 M. Segado, I. Gómez and M. Reguero, Intramolecular charge transfer in aminobenzonitriles and tetrafluoro counterparts: fluorescence explained by competition between low-lying excited states and radiationless deactivation. Part I: A mechanistic overview of the parent system ABN, *Phys. Chem. Chem. Phys.*, 2016, **18**, 6861–6874.

33 M. Lv, X. Wang, D. Wang, X. Li, Y. Liu, H. Pan, S. Zhang, J. Xu and J. Chen, Unravelling the role of charge transfer state during ultrafast intersystem crossing in compact organic chromophores, *Phys. Chem. Chem. Phys.*, 2021, **23**, 25455–25466.

34 K. Chen, I. V. Kurganskii, X. Zhang, A. Elmali, J. Zhao, A. Karatay and M. V. Fedin, Intersystem Crossing and Electron Spin Selectivity in Anthracene-Naphthalimide Compact Electron Donor-Acceptor Dyads Showing Different Geometry and Electronic Coupling Magnitudes, *Chem. – Eur. J.*, 2021, **27**, 7572–7587.

35 Y. Hou, J. Liu, N. Zhang and J. Zhao, Long-Lived Local Triplet Excited State and Charge Transfer State of 4,4′-Dimethoxy Triphenylamine-BODIPY Compact Electron Donor/Acceptor Dyads, *J. Phys. Chem. A*, 2020, **124**, 9360–9374.

36 J. Choi, D.-S. Ahn, K. Y. Oang, D. W. Cho and H. Ihee, Charge Transfer-Induced Torsional Dynamics in the Excited State of 2,6-Bis(diphenylamino)anthraquinone, *J. Phys. Chem. C*, 2017, **121**, 24317–24323.

37 J. Pina, J. S. Seixas de Melo, R. M. F. Batista, S. P. G. Costa and M. M. M. Raposo, Triphenylamine–Benzimidazole Derivatives: Synthesis, Excited-State Characterization, and DFT Studies, *J. Org. Chem.*, 2013, **78**, 11389–11395.

38 M. Heller and U. S. Schubert, Syntheses of Functionalized 2,2′:6′,2″-Terpyridines, *Eur. J. Org. Chem.*, 2003, 947–961.

39 S. S. M. Fernandes, M. Belsley, C. Ciarrocchi, M. Licchelli and M. M. M. Raposo, Terpyridine derivatives functionalized with (hetero)aromatic groups and the corresponding Ru complexes: Synthesis and characterization as SHG chromophores, *Dyes Pigm.*, 2018, **150**, 49–58.

40 C. Wei, Y. He, X. Shi and Z. Song, Terpyridine-metal complexes: Applications in catalysis and supramolecular chemistry, *Coord. Chem. Rev.*, 2019, **385**, 1–19.

41 R. R. Panicker and A. Sivaramakrishna, Remarkably flexible 2,2′:6′,2″-terpyridines and their group 8–10 transition metal complexes – Chemistry and applications, *Coord. Chem. Rev.*, 2022, **459**, 214426.

42 A. M. W. Cargill Thompson, The synthesis of 2,2′:6′,2″-terpyridine ligands—versatile building blocks for supramolecular chemistry, *Coord. Chem. Rev.*, 1997, **160**, 1–52.

43 E. U. Mughal, M. Mirzaei, A. Sadiq, S. Fatima, A. Naseem, N. Naeem, N. Fatima, S. Kausar, A. A. Altaf, M. N. Zafar and B. A. Khan, Terpyridine-metal complexes: effects of different substituents on their physico-chemical properties and density functional theory studies, *R. Soc. Open Sci.*, 2020, **7**, 201208.

44 H. Hofmeier and U. S. Schubert, Recent developments in the supramolecular chemistry of terpyridine–metal complexes, *Chem. Soc. Rev.*, 2004, **33**, 373–399.

45 R. Musiol, P. Malecki, M. Pacholczyk and J. Mularski, Terpyridines as promising antitumor agents: an overview of their discovery and development, *Expert Opin. Drug Discovery*, 2022, **17**, 259–271.

46 I. Eryazici, C. N. Moorefield and G. R. Newkome, Square-Planar Pd(II), Pt(II), and Au(III) Terpyridine Complexes: Their Syntheses, Physical Properties, Supramolecular Constructs, and Biomedical Activities, *Chem. Rev.*, 2008, **108**, 1834–1895.

47 L. M. Hight, M. C. McGuire, Y. Zhang, M. A. Bork, P. E. Fanwick, A. Wasserman and D. R. McMillin, π Donation and Its Effects on the Excited-State Lifetimes of Luminescent Platinum(II) Terpyridine Complexes in Solution, *Inorg. Chem.*, 2013, **52**, 8476–8482.

48 P. Pal, S. Mukherjee, D. Maity and S. Baitalik, Synthesis, Photophysics, and Switchable Luminescence Properties of a New Class of Ruthenium(II)–Terpyridine Complexes Containing Photoisomerizable Styrylbenzene Units, *ACS Omega*, 2018, **3**, 14526–14537.
49 J. Kübel, R. Schroot, M. Wächtler, U. S. Schubert, B. Dietzek and M. Jäger, Photoredox-active Dyads Based on a Ru(II) Photosensitizer Equipped with Electron Donor or Acceptor Polymer Chains: A Spectroscopic Study of Light-Induced Processes toward Efficient Charge Separation, *J. Phys. Chem. C*, 2015, **119**, 4742–4751.
50 M. Maestri, N. Armaroli, V. Balzani, E. C. Constable and A. M. W. C. Thompson, Complexes of the Ruthenium(II)-2,2':6',2''-terpyridine Family. Effect of Electron-Accepting and -Donating Substituents on the Photophysical and Electrochemical Properties, *Inorg. Chem.*, 1995, **34**, 2759–2767.
51 A. M. Maroń, A. Szlapa-Kula, M. Matussek, R. Kruszynski, M. Siwy, H. Janeczek, J. Grzelak, S. Maćkowski, E. Schab-Balcerzak and B. Machura, Photoluminescence enhancement of Re(I) carbonyl complexes bearing D–A and D–π–A ligands, *Dalton Trans.*, 2020, **49**, 4441–4453.
52 A. K. Pal and G. S. Hanan, Design, synthesis and excited-state properties of mononuclear Ru(II) complexes of tridentate heterocyclic ligands, *Chem. Soc. Rev.*, 2014, **43**, 6184–6197.
53 E. A. Medlycott and G. S. Hanan, Designing tridentate ligands for ruthenium(II) complexes with prolonged room temperature luminescence lifetimes, *Chem. Soc. Rev.*, 2005, **34**, 133–142.
54 L. Xiao, Y. Xu, M. Yan, D. Galipeau, X. Peng and X. Yan, Excitation-Dependent Fluorescence of Triphenylamine-Substituted Tridentate Pyridyl Ruthenium Complexes, *J. Phys. Chem. A*, 2010, **114**, 9090–9097.
55 R. Siebert, A. Winter, M. Schmitt, J. Popp, U. S. Schubert and B. Dietzek, Light-Induced Dynamics in Conjugated Bis(terpyridine) Ligands – A Case Study Toward Photoactive Coordination Polymers, *Macromol. Rapid Commun.*, 2012, **33**, 481–497.
56 R. Fernández-Terán and L. Sévery, Living Long and Prosperous: Productive Intraligand Charge-Transfer States from a Rhenium(I) Terpyridine Photosensitizer with Enhanced Light Absorption, *Inorg. Chem.*, 2021, **60**, 1334–1343.
57 R. J. Fernández-Terán and L. Sévery, Coordination Environment Prevents Access to Intraligand Charge-Transfer States through Remote Substitution in Rhenium(I) Terpyridinedicarbonyl Complexes, *Inorg. Chem.*, 2021, **60**, 1325–1333.
58 R. Siebert, A. Winter, U. S. Schubert, B. Dietzek and J. Popp, Excited-State Planarization as Free Barrierless Motion in a π-Conjugated Terpyridine, *J. Phys. Chem. C*, 2010, **114**, 6841–6848.
59 R. Siebert, D. Akimov, M. Schmitt, A. Winter, U. S. Schubert, B. Dietzek and J. Popp, Spectroscopic Investigation of the Ultrafast Photoinduced Dynamics in π-Conjugated Terpyridines, *Chem. Phys. Chem.*, 2009, **10**, 910–919.
60 A. M. Maroń, O. Cannelli, E. C. Socie, P. Lodowski and B. Machura, Push-Pull Effect of Terpyridine Substituted by Triphenylamine Motive—Impact of Viscosity, Polarity and Protonation on Molecular Optical Properties, *Molecules*, 2022, **27**, 7071.
61 E. Socie, B. R. C. Vale, A. Burgos-Caminal and J.-E. Moser, Direct Observation of Shallow Trap States in Thermal Equilibrium with Band-Edge Excitons in Strongly Confined CsPbBr3 Perovskite Nanoplatelets, *Adv. Opt. Mater.*, 2021, **9**, 2001308.
62 A. M. Maroń, K. Choroba, T. Pedzinski and B. Machura, Towards better understanding of the photophysics of platinum(II) coordination compounds with anthracene- and pyrene-substituted 2,6-bis(thiazol-2-yl)pyridines, *Dalton Trans.*, 2020, **49**, 13440–13448.
63 C. Slavov, H. Hartmann and J. Wachtveitl, Implementation and Evaluation of Data Analysis Strategies for Time-Resolved Optical Spectroscopy, *Anal. Chem.*, 2015, **87**, 2328–2336.
64 W. Kohn and L. J. Sham, Self-Consistent Equations Including Exchange and Correlation Effects, *Phys. Rev.*, 1965, **140**, A1133–A1138.
65 E. Runge and E. K. U. Gross, Density-Functional Theory for Time-Dependent Systems, *Phys. Rev. Lett.*, 1984, **52**, 997–1000.
66 C. Adamo and V. Barone, Toward reliable density functional methods without adjustable parameters: The PBE0 model, *J. Chem. Phys.*, 1999, **110**, 6158–6170.
67 M. Ernzerhof and G. E. Scuseria, Assessment of the Perdew–Burke–Ernzerhof exchange-correlation functional, *J. Chem. Phys.*, 1999, **110**, 5029–5036.
68 F. Weigend and R. Ahlrichs, Balanced basis sets of split valence, triple zeta valence and quadruple zeta valence quality for H to Rn: Design and assessment of accuracy, *Phys. Chem. Chem. Phys.*, 2005, **7**, 3297–3305.
69 J. Tomasi, B. Mennucci and R. Cammi, Quantum Mechanical Continuum Solvation Models, *Chem. Rev.*, 2005, **105**, 2999–3094.
70 T. Jarusuwannapoom, W. Hongrojjanawiwat, S. Jitjaicham, L. Wannatong, M. Nithitanakul, C. Pattamaprom, P. Koombhongse, R. Rangkupan and P. Supaphol, Effect of solvents on electro-spinnability of polystyrene solutions and morphological appearance of resulting electrospun polystyrene fibers, *Eur. Polym. J.*, 2005, **41**, 409–421.
71 T. Dong, E. P. Knoshaug, P. T. Pienkos and L. M. L. Laurens, Lipid recovery from wet oleaginous microbial biomass for biofuel production: A critical review, *Appl. Energy*, 2016, **177**, 879–895.
72 D. S. Gill and D. Rana, Preparation of Some Novel Copper(I) Complexes and their Molar Conductances in Organic Solvents, *Z. Naturforsch., A: Phys. Sci.*, 2009, **64**, 269–272.
73 A. S. R. Koti, M. M. G. Krishna and N. Periasamy, Time-Resolved Area-Normalized Emission Spectroscopy (TRANES): A Novel Method for Confirming Emission from Two Excited States, *J. Phys. Chem. A*, 2001, **105**, 1767–1771.
74 A. S. R. Koti and N. Periasamy, Application of time resolved area normalized emission spectroscopy to multicomponent systems, *J. Chem. Phys.*, 2001, **115**, 7094–7099.
75 K. Ramamurthy, K. Ponnusamy and S. Chellappan, Excitation-resolved area-normalized emission spectroscopy:

a rapid and simple steady-state technique for the analysis of heterogeneous fluorescence, *RSC Adv.*, 2020, **10**, 998–1006.

76 A. Cesaretti, B. Carlotti, P. L. Gentili, R. Germani, A. Spalletti and F. Elisei, Twisting in the excited state of an N-methylpyridinium fluorescent dye modulated by nano-heterogeneous micellar systems, *Photochem. Photobiol. Sci.*, 2016, **15**, 525–535.

77 B. Carlotti, A. Cesaretti, C. G. Fortuna, A. Spalletti and F. Elisei, Experimental evidence of dual emission in a negatively solvatochromic push–pull pyridinium derivative, *Phys. Chem. Chem. Phys.*, 2015, **17**, 1877–1882.

78 B. Carlotti, E. Benassi, A. Cesaretti, C. G. Fortuna, A. Spalletti, V. Barone and F. Elisei, An ultrafast spectroscopic and quantum mechanical investigation of multiple emissions in push–pull pyridinium derivatives bearing different electron donors, *Phys. Chem. Chem. Phys.*, 2015, **17**, 20981–20989.

79 M. L. Horng, J. A. Gardecki, A. Papazyan and M. Maroncelli, Subpicosecond Measurements of Polar Solvation Dynamics: Coumarin 153 Revisited, *J. Phys. Chem.*, 1995, **99**, 17311–17337.

80 C. Bonaccorso, A. Cesaretti, F. Elisei, L. Mencaroni, A. Spalletti and C. G. Fortuna, New Styryl Phenanthroline Derivatives as Model D−π−A−π−D Materials for Non-Linear Optics, *Chem. Phys. Chem.*, 2018, **19**, 1917–1929.

81 A. El Nahhas, A. Cannizzo, F. van Mourik, A. M. Blanco-Rodríguez, S. Záliš, A. Vlček and M. Chergui, Ultrafast Excited-State Dynamics of [Re(L)(CO)3(bpy)] n Complexes: Involvement of the Solvent, *J. Phys. Chem. A*, 2010, **114**, 6361–6369.

82 A. El Nahhas, C. Consani, A. M. Blanco-Rodríguez, K. M. Lancaster, O. Braem, A. Cannizzo, M. Towrie, I. P. Clark, S. Záliš, M. Chergui and A. Vlček, Ultrafast Excited-State Dynamics of Rhenium(I) Photosensitizers [Re(Cl)(CO)3-(N,N)] and [Re(imidazole)(CO)3(N,N)] +: Diimine Effects, *Inorg. Chem.*, 2011, **50**, 2932–2943.

83 Q. Sun, S. Mosquera-Vazquez, L. M. Lawson Daku, L. Guénée, H. A. Goodwin, E. Vauthey and A. Hauser, Experimental Evidence of Ultrafast Quenching of the ^{3} MLCT Luminescence in Ruthenium(II) Tris-bipyridyl Complexes via a ^{3} dd State, *J. Am. Chem. Soc.*, 2013, **135**, 13660–13663.

84 A. N. Tarnovsky, W. Gawelda, M. Johnson, C. Bressler and M. Chergui, Photexcitation of Aqueous Ruthenium(II)-tris-(2,2'-bipyridine) with High-Intensity Femtosecond Laser Pulses, *J. Phys. Chem. B*, 2006, **110**, 26497–26505.

85 M. R. Son, Y.-J. Cho, S.-Y. Kim, H.-J. Son, D. W. Cho and S. O. Kang, Direct observation of the photoinduced electron transfer processes of bis(4-arylphenylamino benzo)-ortho-carborane using transient absorption spectroscopic measurements, *Phys. Chem. Chem. Phys.*, 2017, **19**, 24485–24492.

86 B. Carlotti, G. Consiglio, F. Elisei, C. G. Fortuna, U. Mazzucato and A. Spalletti, Intramolecular Charge Transfer of Push–Pull Pyridinium Salts in the Singlet Manifold, *J. Phys. Chem. A*, 2014, **118**, 3580–3592.

